Supporting Information

Favoring photocatalytic reactive species generation and utilization over g-C_3N_4 nanosheets by controllable edge C modification

Tingshuo Ji[a,b,#], Yangyang Liu[a,#], Peng Jin[c], Xue Wei[a,b], Xuetong Li[a], Shouren Zhang[a], Xuefeng Wei[b,*], Baocheng Yang[a,*], Yanzhen Guo[a,*]

[a]Henan Provincial Key Laboratory of Nanocomposites and Applications, Institute of Nanostructured Functional Materials, Huanghe Science and Technology College, Zhengzhou 450006, China. E-mail: yzguo@hhstu.edu.cn; baochengyang@infm.hhstu.edu.cn
[b]College of Chemical Engineering & Pharmaceutics, Henan University of Science and Technology, Luoyang, 471023, PR China. E-mail: xfwei@haust.edu.cn
[c]State Key Laboratory of Coking Coal Exploitation and Comprehensive Utilization, China Pingmei Shenma Group, Pingdingshan 467000, China
#The authors contribute equally.

Density functional theory (DFT) calculations

The structural optimization was carried out by Vienna *Ab-initio* Simulation Package(VASP)[S1] with the projector augmented wave (PAW) method.[S2] The exchange-correlation functional was treated using the Perdew-Burke-Ernzerhof (PBE)[S3] functional in combination with the DFT-D3 correction.[S4] The cut-off energy of the plane-wave basis was set at 450 eV. For the optimization of both geometry and lattice size, the Brillouin zone integration is performed with 2×2×1 Monkhorst[S5] *k*-point sampling. The self-consistent calculations applied a convergence energy threshold of 10^{-5} eV. The equilibrium geometries and lattice constants were optimized with maximum stress on each atom within 0.02 eV/Å. In calculation of band structure, high-symmetry points were obtained by vaspkit interface.[S6,S7]

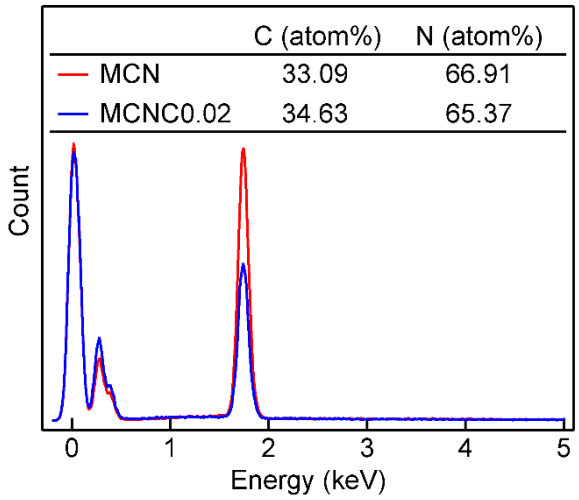

Fig. S1 The EDX spectra and element content of MCN and MCNC0.02.

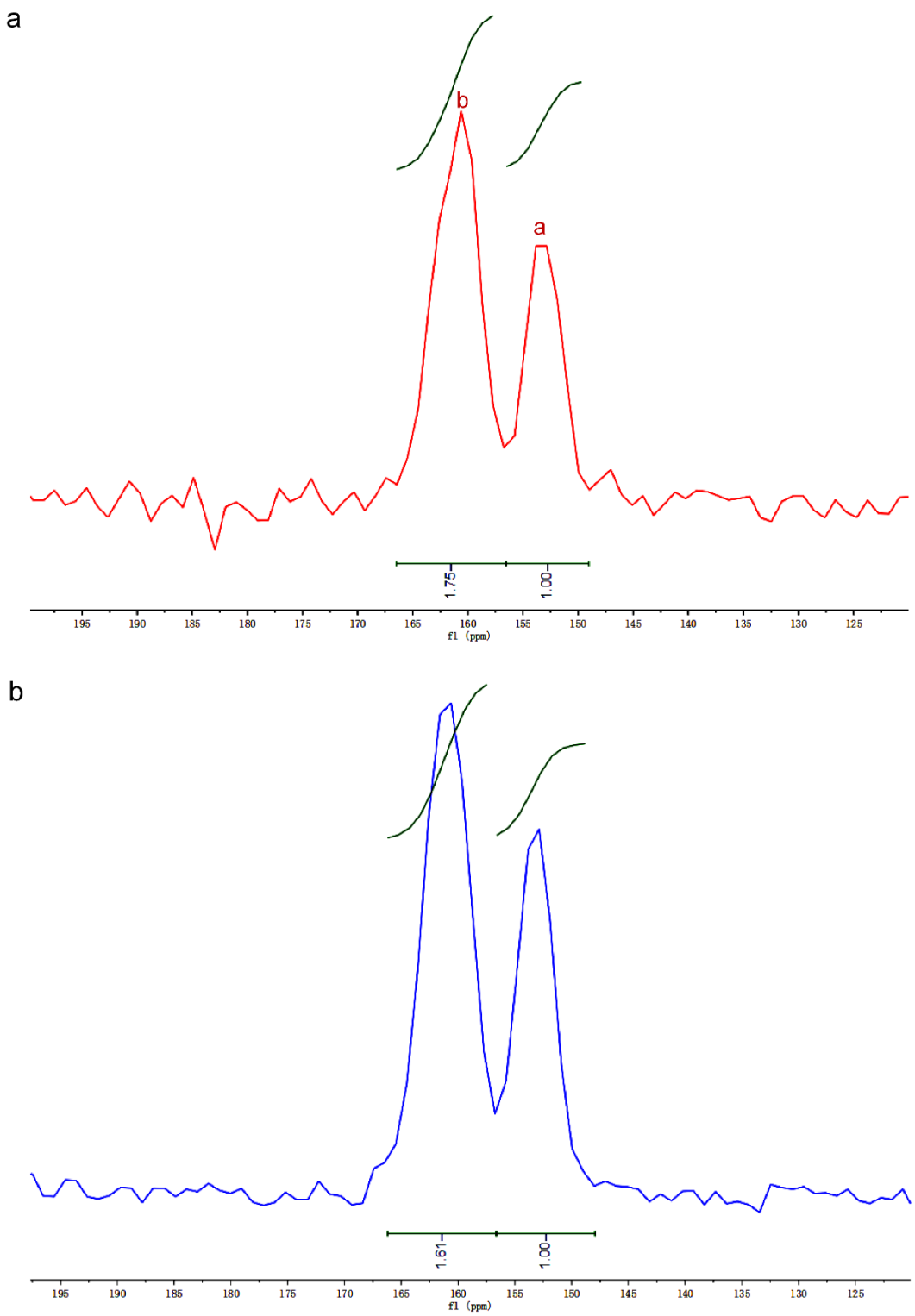

Fig. S2 The solid-state ^{13}C NMR spectra of MCN (a) and MCNC0.02 (b).

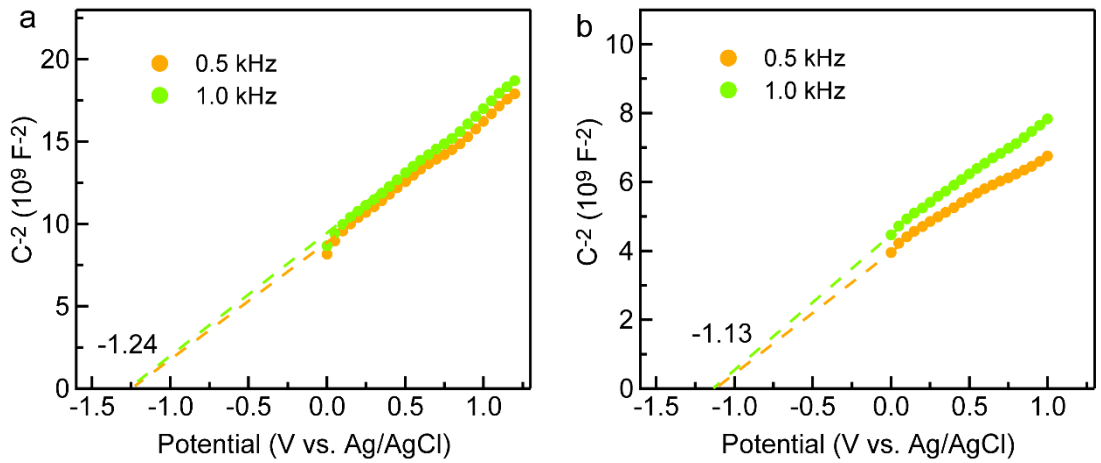

Fig. S3 The Mott–Schottky curves of MCN (a) and MCNC0.02 (b).

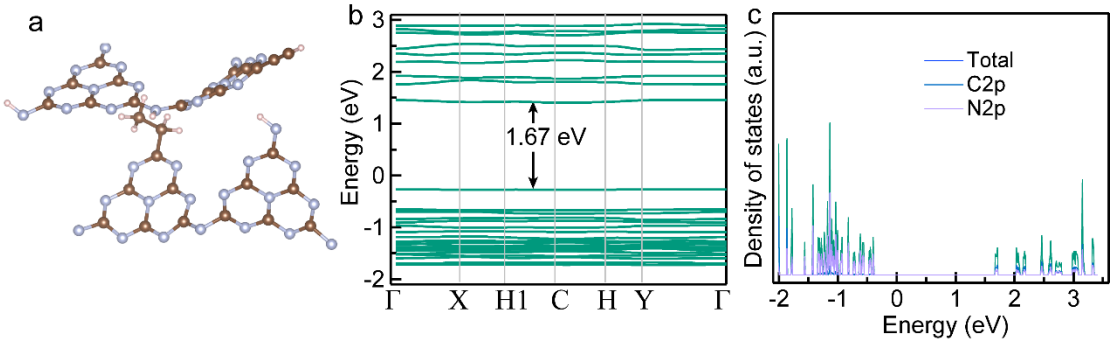

Fig. S4 DFT calculations of the methyl/acetenyl modified g-C_3N_4. (a) Structure model. (b) Band structure. (c) Density of states.

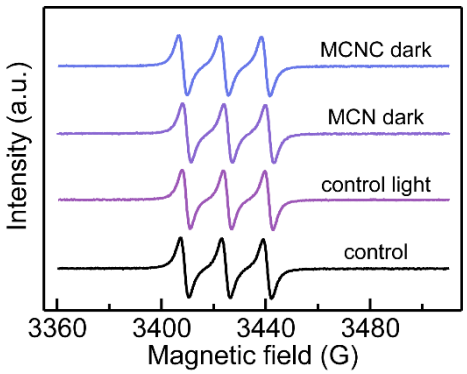

Fig. S5 EPR spectra of the control samples using TEMPO as the spinning probe.

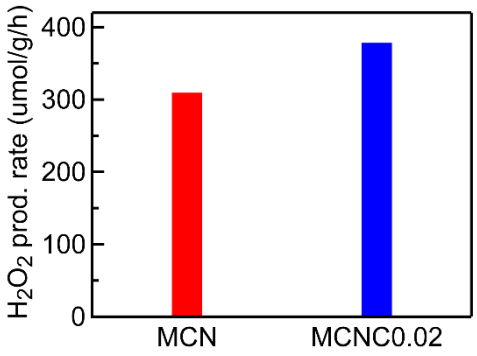

Fig. S6 Photocatalytic H_2O_2 generation rate of MCN and MCNC0.02.

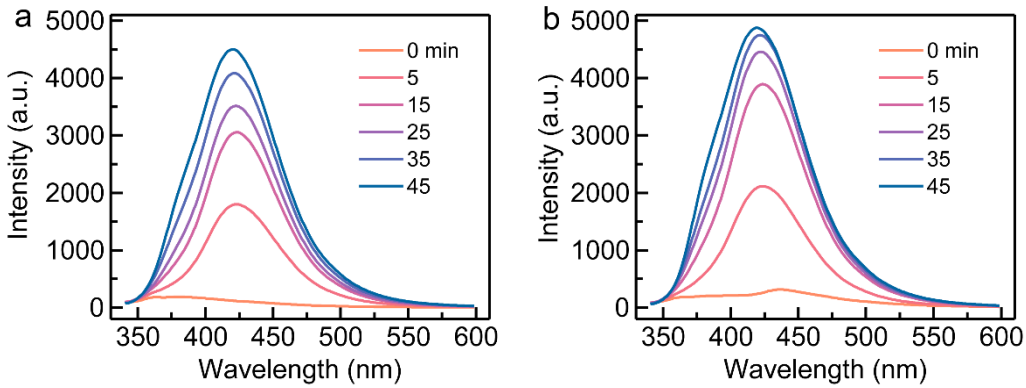

Fig. S7 Detection of •OH by using TA as a fluorescent probe. (a) MCN, (b) MCNC.

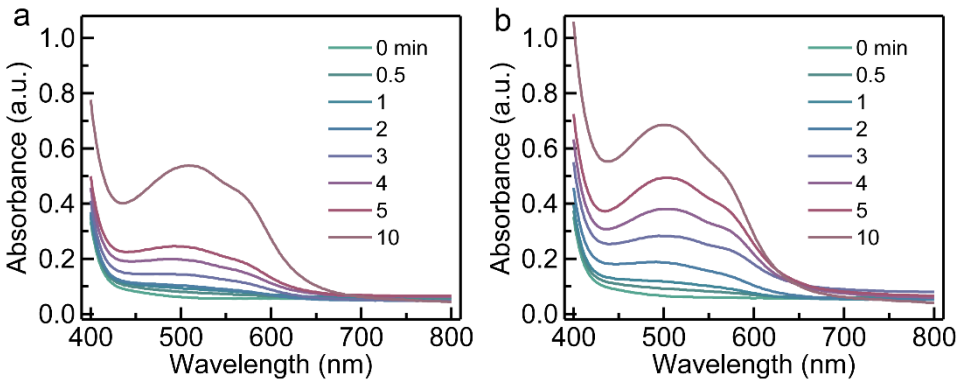

Fig. S8 Detection of $\bullet O_2^-$ by using INT as a probe molecule. (a) MCN, (b) MCNC.

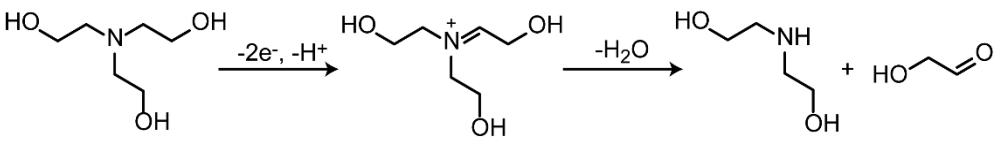

Fig. S9 The proposed oxidation path of TEOA according to previous reports.[S8]

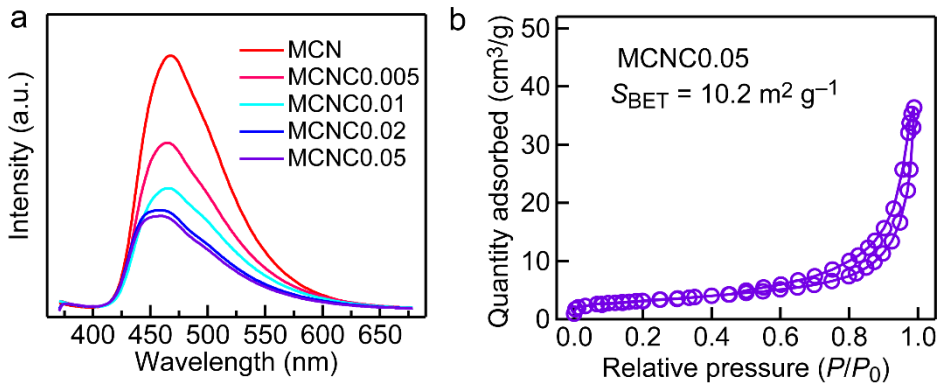

Fig. S10 The characterizations of the C-doped g-C_3N_4 samples. (a) Steady-state PL spectra of the pristine and C-modified g-C_3N_4 samples. (b) N_2 adsorption-desorption isothermal curve of MCNC005.

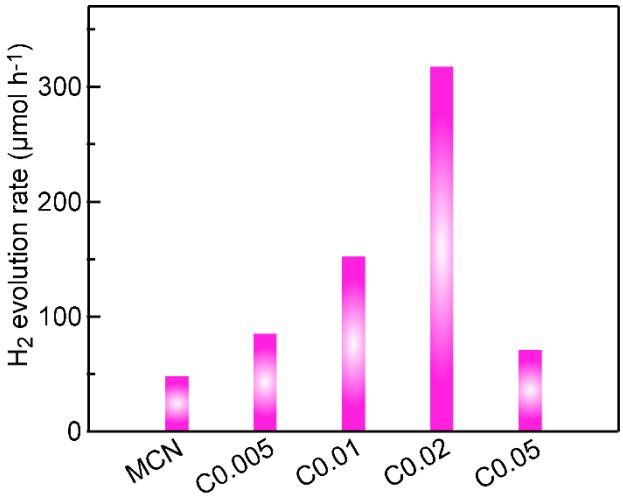

Fig. S11 Photocatalytic hydrogen evolution of the samples under white light irradiation.

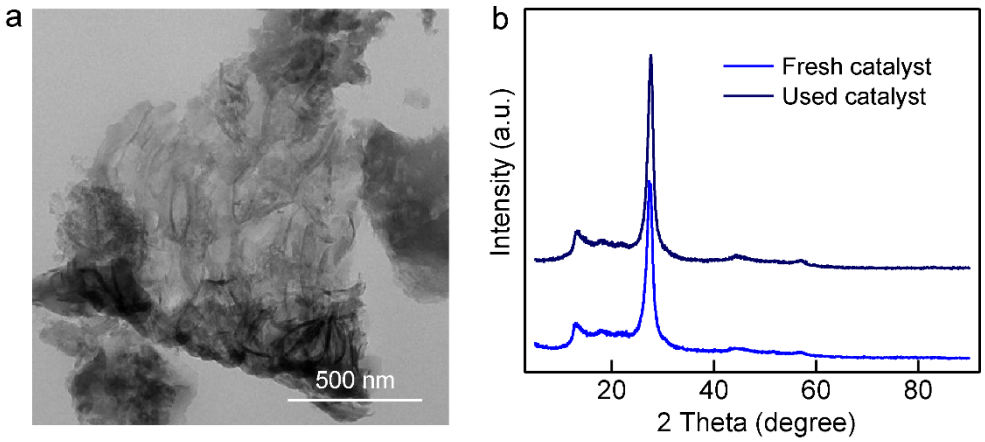

Fig. S12 The characterizations of the samples after stability test. (a) TEM image of MCNC0.02 after cyclic test. (b) XRD patterns of the fresh and used MCNC0.02 sample.

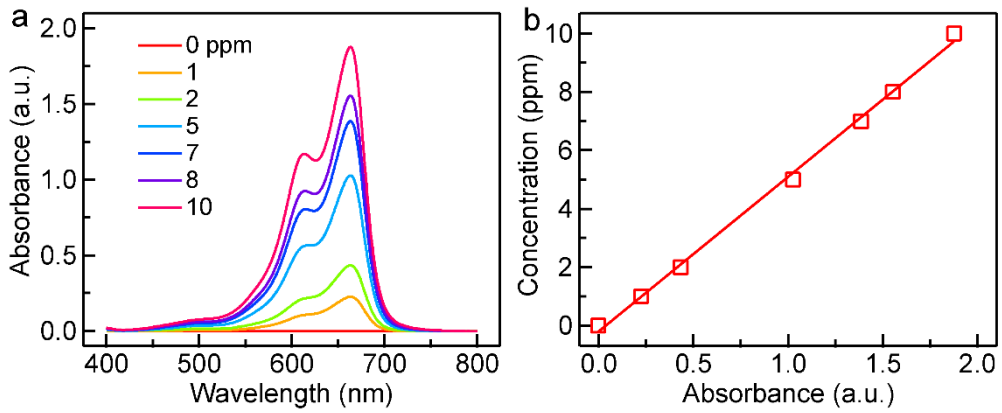

Fig. S13 The calibration curves for the measurement of MB concentration. (a) Absorbance curves of MB with different concentrations. (b) Calibration curve of MB by monitoring the wavelength at 664 nm.

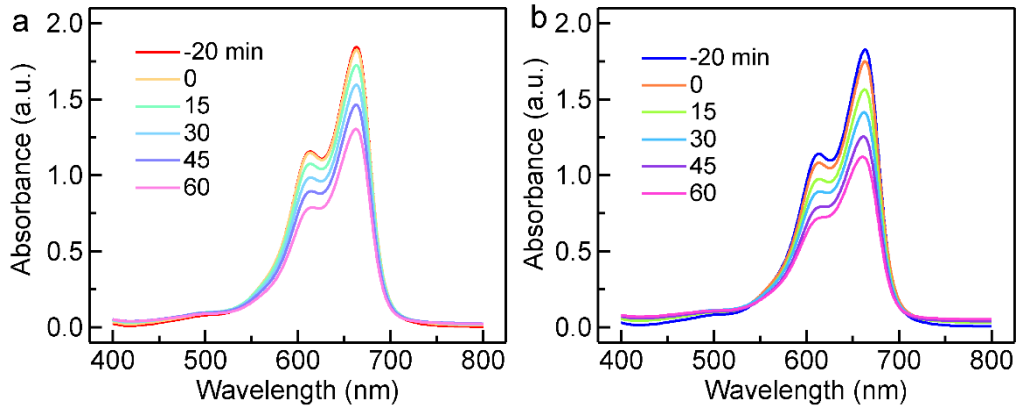

Fig. S14 The photocatalytic MB degradation of the samples under visible light ($\lambda >$ 420 nm) irradiation. (a) MCN. (b) MCNC0.02.

Table S1 Elemental analysis of the MCN and MCNC samples.

Atomic ratio (%) / Samples	C	N
MCN	32.13	67.87
MCNC	34.92	65.08

Table S2 Comparison of the H_2 evolution rate and AQY values over some g-C_3N_4-based photocatalysts.

Photocatalyst	Light source	Co-catalyst	Sacrificial agent	H_2 evolution rate (μmol g^{-1} h^{-1})	AQY	Ref.
g-C_3N_4	300 W Xe lamp, λ > 420 nm	Pt (3.0 wt%)	TEOA (10 vol%)	106.9	/	S9
Polytriazine imide/Li^+Cl^-	300 W Xe lamp, λ > 300 nm	Pt (1.0 wt%)	Overall water splitting	1890.0	~6.0% at 380 nm	S10
Triptycene incorporated g-C_3N_4	300 W Xe lamp, λ > 420 nm	Pt (1.0 wt%)	TEOA (10 vol%)	1618.0	4.8% at 420 nm	S11
C-incorporated g-C_3N_4	300 W Xe lamp, λ > 420 nm	Pt (0.5 wt%)	TEOA (15 vol%)	2500.0	/	S12
C bridged g-C_3N_4	300 W Xe lamp, λ > 420 nm	Pt (3.0 wt%)	TEOA (10 vol%)	529.0	/	S13
Holey C-doped g-C_3N_4	Medium pressure mercury, λ > 400 nm	Pt (3.0 wt%)	EDTA (10 vol%)	60.9	2.05% at 417 nm, 0.88% at 458 nm	S14
Ascorbic acid modified g-C_3N_4	300 W Xe lamp, λ > 400 nm	Pt (1.0 wt%)	TEOA (10 vol%)	198.2	/	S15
C-doped g-C_3N_4	500 W Xe lamp, AM 1.5G, 100 mW cm^{-2}	Pt (1.0 wt%)	Methanol (10 vol%)	216.8	/	S16
C-doped g-C_3N_4@C, N co-doped ZnO	500 W Xe lamp, AM 1.5G, 100 mW cm^{-2}	Pt (1.0 wt%)	Methanol (10 vol%)	441.4	/	S17
C-incorporated g-C_3N_4	300 W Xe lamp, λ > 420 nm	Pt (3.0 wt%)	TEOA (10 vol%)	1003.9	/	S18
Porous C-doped C_3N_4	300 W Xe lamp, λ > 420 nm	Pt (3.0 wt%)	TEOA (20 vol%)	1266.8	10.1% at 420 nm	S19
C self-doped	300 W Xe	Pt (3.0	TEOA (10	1224.0	/	S20

g-C_3N_4	lamp, λ > 400 nm	wt%)	vol%)			
C-enriched porous g-C_3N_4	300 W Xe lamp, λ > 420 nm	Pt (3.0 wt%)	TEOA (10 vol%)	2352.0	/	S21
Broom-like O-doped g-C_3N_4	300 W Xe lamp, λ > 420 nm	Pt (3.0 wt%)	TEOA (10 vol%)	13610.0	/	S22
Edge C-modified g-C_3N_4	300 W Xe lamp, λ > 420 nm	Pt (3.0 wt%)	TEOA (10 vol%)	626.0	5.0% at 380 nm, 1.9% at 420 nm, 1.1% at 450 nm	This work

Reference

S1 J. Hafner, *J. Comput. Chem.*, 2008, **29**, 2044–2078.

S2 P. E. Blöchl, *Phys. Rev. B*, 1994, **50**, 17953.

S3 J. P. Perdew, K. Burke, M. Ernzerhof, *Phys. Rev. Lett.*, 1996, **77**, 3865.

S4 S. Grimme, *J. Comput. Chem.*, 2006, **27**, 1787–1799.

S5 H. J. Monkhorst, J. D. Pack., *Phys. Rev. B*, 1976, **13**, 5188.

S6 V. Wang, N. Xu, J.-C. Liu, G. Tang, W.-T. Geng, *Comput. Phys. Commun.*, 2021, **267**, 108033.

S7 V. Wang, G. Tang, R.-T. Wang, Y.-C. Liu, H. Mizuseki, Y. Kawazoe, J. Nara, W.-T. Geng, arXiv:1806.04285.

S8 O. Savateev, Y. J. Zou, *ChemistryOpen*, 2022, **11**, e202200095.

S9 X. C. Wang, K. Maeda, A. Thomas, K. Takanabe, G. Xin, J. M. Carlsson, K. Domen, M. Antonietti, *Nat. Mater.*, 2009, **8**, 76–80.

S10 L. H. Lin, Z. Y. Lin, J. Zhang, X. Cai, W. Lin, Z. Y. Yu, X. C. Wang, *Nat. Catal.*, 2020, **3**, 649–655.

S11 Y. Zheng, L. L. Zhan, Y. K. Li, Y. Y. Wang, J. L. Chen, B. Z. Lin, Y. Z. Zheng, Cheng, S. B. Wang, Y. L. Chen, *J. Colloid Interface Sci.*, 2022, **622**, 675–689.

S12 J. Li, D. D. Wu, J. Iocozzia, H. W. Du, X. Q. Liu, Y. P. Yuan, W. Zhou, Z. Li, Z. M. Xue, Z. Q. Lin, *Angew. Chem. Int. Ed.*, 2019, **58**, 1985–1989.

S13 H. L. Li, F. P. Li, Z. Y. Wang, Y. C. Jiao, Y. Y. Liu, P. Wang, X. Y. Zhang, X. Y. Qin, Y. Dai, B. B. Huang, *Appl. Catal., B*, 2018, **229**, 114–120.

S14 E. S. D. Silva, N. M. M. Moura, A. Coutinho, G. Dražić, B. M. S. Teixeira, N. A. Sobolev, C. G. Silva, M. G. P. M. S. Neves, M. Prieto, J. L. Faria, *ChemSusChem*, 2018, **11**, 2681–2694.

S15 R. C. Pawar, S. Kang, H. Han, H. Choi, C. S. Lee, *Catal. Sci. Technol.*, 2019, **9**, 1004–1012.

S16 M. A. Mohamed, M.F. M. Zain, L. J. Minggu, M. B. Kassim, J. Jaafar, N. A. S. Amin, Z. A. M. Hir, M. S. Rosmi, *Int. J. Hydrogen Energy*, 2019, **44**, 13098–13105.

S17 M. A. Mohamed, M.F. M. Zain, L. J. Minggua, M. B. Kassim, J. Jaafar, N. Aishah S. Amine, M. S. Mastuli, H. Wu, R. J. Wong, Y. H. Ng, *J. Ind. Eng. Chem.*, 2019, **77**, 393–407.

S18 Y. Y. Huang, D. Li, Z. Y. Fang, R. J. Chen, B. F. Luo, W. D. Shi, *Appl. Catal., B*, 2019, **254**, 128–134.

S19 Y. B. Jiang, Z. G. Lin, Y. Y. Zhang, Y. C. Lai, D. Liang, C. Z. Yang, *New J. Chem.*, 2020, **44**, 17891–17898.

S20 E. L. Liu, X. Lin, Y. Z. Hong, L. Yang, B. F. Luo, W. L. Shi, J. Y. Shi, *Renewable Energy*, 2021, **178**, 757–765.

S21 J. Q. Wen, Y. W. Wang, H. Zhao, M. Zhang, S. Y. Zhang, Y. G. Liu, Y. P. Zhai, *New J. Chem.*, 2022, **46**, 4647–4653.

S22 Y. R. Shang, Y. Wang, C. D. Lv, F. Y. Jing, T. X. Liu, W. L. Li, S. S. Liu, G. Chen, *Chem. Eng. J.*, 2022, **431**, 133898.